

X-ray performance of gratings in the extreme off-plane mount

Randall L. McEntaffer^{*a}, Steven Osterman^a, Webster Cash^a, John Gilchrist^b, Jean Flamand^c,
Bruno Touzet^c, Francis Bonnemason^c, Christian Brach^c

^aUniversity of Colorado, Center for Astrophysics and Space Astronomy, 593 UCB,
1255 38th St, Boulder, CO 80309-0593;

^bJobin-Yvon Inc., 3880 Park Avenue, Edison, New Jersey 08820-3012

^cJobin-Yvon SAS, 16-18 rue du Canal, Longjumeau, France 91160

Abstract

High groove density reflection gratings placed at grazing incidence in the extreme off-plane mount offer increased performance over conventional in-plane mounts in the x-ray. We present initial off-plane efficiency test results from the grating evaluation facility at the University of Colorado. The test gratings are holographically ruled, ion-etched gratings with radial groove profiles that were developed and fabricated by Jobin-Yvon Inc.

Keywords: Off-plane mount, holographic grating

1. Introduction

1.1 Constellation-X

The Constellation-X mission will provide an instrument with large effective collecting area and high spectral resolution relative to past and current x-ray observatories. An overview of the mission and science goals is given by Tananbaum, et al.¹, and can be found on the web at <http://constellation.gsfc.nasa.gov>.

Briefly, the mission incorporates three instruments, all designed to perform high throughput spectroscopy of astronomical x-ray sources. For x-ray energies above 10keV there is a hard x-ray telescope (HXT) and from 0.1 to 10keV, there is a large foil optic telescope known as the SXT. The SXT has its light divided between two instruments – a calorimeter and a reflection grating spectrometer (RGS). The calorimeter is optimized for spectroscopy from 1 to 10keV, and the reflection gratings are optimized for the softest x-rays, 0.2 - 1keV where the performance of the calorimeter falls off.

The RGS will use dispersive spectroscopy to provide high resolution at the long wavelength end of the x-ray spectrum. In order to achieve the high spectral resolution and effective area required of the Constellation-X mission we propose using a high density, radial groove grating array in the off-plane mount. This system could potentially reach resolution ($\lambda/\Delta\lambda$) of 5000 and effective area >3000cm² as described in McEntaffer et al².

1.2 Off-plane geometry

The off-plane mount at grazing incidence brings light onto the grating at a low graze angle, quasi-parallel to the direction of the grooves as shown in figure 1^{3,4}. The light is then diffracted through an arc, forming a cone, so that this mount is also known as conical diffraction. The grating equation is now

$$\sin\alpha + \sin\beta = \frac{n\lambda}{d\sin\gamma}. \quad (1)$$

* randy@origins.colorado.edu; phone 1 303 492-5835; fax 1 303 492-5941; <http://casa.colorado.edu>; Center for Astrophysics and Space Astronomy, Astrophysics Research Laboratory, 593 UCB, 1255 38th Street, Boulder, CO, USA 80309-0593

where d is the spacing between grooves. γ is the angle between the direction of the incoming ray and the direction of the groove at the point of impact. Light comes into the grating at an azimuthal angle of α along a cone with half-angle γ . It is then diffracted along the same cone of half-angle γ , but now with an azimuthal angle of β .

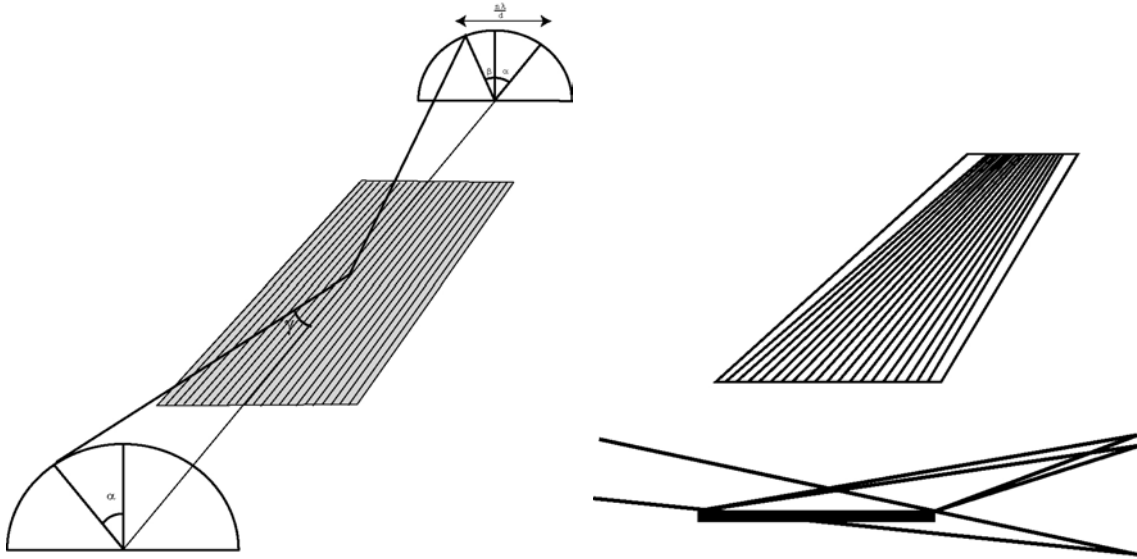


Fig. 1: Geometry of the off-plane mount. Quasi-parallel light at grazing incidence is diffracted in a cone around the direction of the rulings. Off-axis aberrations such as coma can be corrected using a radial groove grating in the converging beam.

When the gratings are placed behind the optics, the off-axis aberrations are corrected if the gratings compensate for the converging beam of the telescope. This can be done by using gratings that are ruled in a radial configuration where the grooves extend outward from a hub and match the convergence angle of the beam as shown in figure 1.

The off-plane mount supplies the natural geometry for grazing incidence reflection gratings, thus offering several advantages of which diffraction efficiency is key. The effective diffraction efficiency of the off-plane mount can be substantially higher than traditional mounts (often a factor of two) due to the groove illumination function^{5,6}. In the off-plane mount the effect of groove shadowing is lessened. Furthermore, rigorous efficiency calculations of blazed gratings show that the off-plane mount can have efficiencies up to 70% and on average a few times higher than efficiencies obtainable with a traditional in-plane grating mount⁷. We present here first results on the efficiencies of Constellation-X RGS prototype gratings operating in the off-plane mount.

2. Methodology

2.1 Grating Fabrication

A review of the state of the art of high ruling-density grating fabrication has been completed. The efficiencies obtained by holographically ruled gratings surpass those that incorporate the conventional machine-ruling. At the onset of the off-plane RGS study several possible grating suppliers were considered. Jobin-Yvon was chosen because of their expertise with high groove density, holographically ruled gratings. The aim of this manufacturing study was to check the feasibility of blazing a high groove density holographically generated grating with a radial groove distribution.

Holographic master gratings are produced by starting with a highly polished and figured substrate in an identical manner to that required for mechanically ruled gratings. However, as opposed to the mechanically ruled gratings where a diamond tool cuts the grooves, holographic gratings are ruled chemically. The blank is coated with a layer of photosensitive material and then exposed to the interference fringes created by the intersection of two coherent laser beams. Chemical treatment of the photoresist layer selectively dissolves the exposed areas forming grooves in relief. The geometry of the laser wavefronts used to produce the interference fringes can be modified to produce either a linear

or non-linear groove distribution on the surface. In general the result of such an exposure is a sinusoidal groove profile, normally referred to as a holographic grating. If this profile is the final requirement the photoresist layer is usually coated with a suitable metallic coating (Au, Pt or Al) determined from the spectral region the grating will be used in. For the work presented here a blazed profile was required and a holographic mask was exposed whose groove shape is non-sinusoidal. This was optimized for the requirements of the ion-etching process and the particular blaze angle required.

Spectral efficiency depends upon the groove profiles that are derived from the recorded holographic mask. Ion etching erosion is used for the “sculpting” of the groove profile into the blank material. The evolution of the groove profile by ion-etching can be described by a faceting model assuming that local erosion rates are a consequence of angular dependence of sputtering yields along the geometrical motif of the holographic mask. Erosion rates can be precisely adjusted by monitoring the ion beam energy and density with respect to the thermal behavior of the photoresist. Groove sculpting can be produced to high levels of accuracy. Once the final profile is obtained in the substrate any residual photoresist that may be left is removed by appropriate chemical treatment.

The groove profile is checked on the grating with an atomic force microscope. Characteristic parameters (height, blaze angle and line spacing) are determined by averaging over several grooves on test grating samples. Uniformity of the sculpting process along the whole surface is ensured by careful adjustment of the interferogram pattern and by careful control of the ion beam section and process optimization. Once in agreement with the requirement, a final (master) grating is made by submitting the blank to the optimized process of holographic recording of the mask and ion etching.

2.2 Test Setup and Data Analysis

The general layout of our test setup consists of a Manson electron impact X-ray source that sends light through an entrance slit to a single-pass off-plane X-ray monochromator that disperses the desired spectral line through an exit slit into the vacuum tank that houses the test grating. For a complete description of the monochromator see McEntaffer et al. in these proceedings⁸. In the vacuum tank there is an aperture stop just before the test grating. Such a slit is important to make certain that the test grating placed at grazing incidence can intersect the entire beam. If the beam is larger than the projected size of the grating then the amount of incident light will be overestimated and measured efficiencies will be less than actual. This stop is a knife-edge slit that can be adjusted to accommodate multiple size gratings but has been kept at $600 \times 1500 \mu\text{m}$ for the tests presented here. It is mounted on two translational stages and one rotational stage. The translation stages optimize the position of the slit relative to the incoming spectral line from the monochromator insuring maximal flux on the test grating. The rotational stage is used to tilt the slit to match the tilt of the test grating. The test grating is controlled over four degrees of freedom by two rotational and two translational stages. The translation stages move the grating in and out of the beam along the grating surface normal or up and down in the plane of the grating. One of the rotational stages rotates the grating about an axis coincident with the central groove of the grating thus tilting the grating by an angle equal to the blaze angle so that the blazed facets are vertical and orders satisfying the blaze constraint will be thrown horizontally. The other rotation is about the vertical axis that passes through the grating center such that any rotation by this stage supplies the angle γ in the grating equation. The swing arm stage that holds the detector also rotates about this axis so that the detector can be slewed across the focal plane to catch the diffracted light as depicted in figure 2.

To begin a data set the appropriate anode, usually carbon, magnesium or copper, is installed in the Manson X-ray source. Then within the vacuum test chamber the test grating and the aperture stop are moved out of the beam path so that light exiting the monochromator is incident on the detector. This allows a complete characterization of the spectrum from the monochromator as described in McEntaffer et

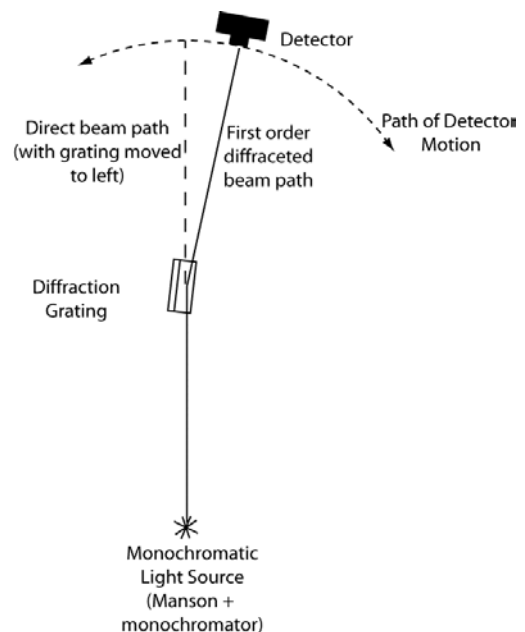


Figure 2: Test setup orientation. The source feeds the test grating via a monochromator and an MCP detector samples the diffraction arc.

al. to obtain a clean, bright line. The aperture stop is then moved into the beam and positioned to sample the center of the spectral line to minimize continuum contamination while maximizing flux. The image resulting at the detector is now the direct beam. Then the test grating position is optimized. First the grating is moved into the direct beam so that it cuts the flux down by a factor of two. This assures that the center of the slit is on the center of the grating given that all grating rotations are about its center. The grating is rotated by a small γ , usually around 0.1 degrees, to produce a double image consisting of zero order and remaining direct flux. The zero order image is then steered back onto the direct beam to make the grating face parallel with the light. The grating is then pulled out of the beam and rotated to 2 degrees. It is then moved into the direct beam until it disappears leaving the slit center 300 μm from the edge. The grating is moved an additional 712 μm into the beam path to position the center of the 58mm grating at 2 degrees coincident with the center of the slit. At this point the detector, which measures 9mm in the horizontal dimension and 60mm in the vertical, is slewed across the diffraction arc. Typically six exposures are needed to capture the entire arc of diffraction. Another direct image and a background exposure are taken to complete the data set. A complete data set is shown in figure 3. Vertical strips of detector area are concatenated together to form this image. On the left is the vertical strip containing the direct image with the test grating out of the beam path. As previously stated the grating is then moved into the beam and the detector moved over to the diffraction arc. The blank area is space between the direct image and the diffraction arc that was not sampled by the detector. The lines on the right display the arc of dispersion as expected from conical diffraction. Lines must be contained completely within one strip as opposed to being created by adding two different strips together if the data are to be accurate. Only the central ~60% of the active area in the horizontal dimension is considered for each strip due to gain variations at the edges. To account for any drift in the source flux, two direct images, taken at the start and end of the data set, are averaged. Boxes are drawn around the direct image, spectral lines and background areas. Background counts per area are calculated from the background boxes to reduce the direct and diffracted data. These numbers are then used to calculate efficiencies:

$$\text{Absolute Efficiency} = (\text{Diffracted Counts} - \text{Background}) / (\text{Direct Counts} - \text{Background})$$

Errors from this method can occur due to detector effects and transient hot spots. Long data sets lead to thermal effects at the detector which materialize as hot spots as well as elongation of saturated areas in the horizontal dimension. Retaking data in which hot spots interfere with spectral lines and minimizing integration times by using high line fluxes are two measures taken to reduce the effects of the detector.

The grating tested here is a holographically ruled radial groove grating designated U3787. The resulting blaze angle is 9.094 degrees with a groove density of 4245 grooves/mm and a 300 \AA platinum coating. Since the light coming from the monochromator is diverging the grooves are placed anti-parallel to the direction they would have in the converging beam of the Constellation-X RGS.

3. Results

Figure 4 shows data taken at the Carbon-K emission line, 0.277keV. The direct beam is box 0, first order is box 1, zero order is box 2 and minus first order is box 3. Recall zero order is at an angle with respect to horizontal because the grating is placed at a tilt so that the blazed facets are vertical and any light satisfying the blaze constraint will be diffracted horizontally. However, there is some error in this positioning because there is no control over the alignment

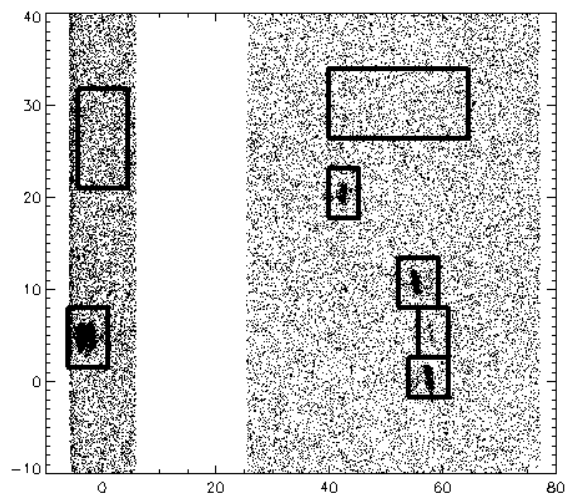


Figure 3: Concatenation of detector scans giving a complete image of the direct beam and the arc of dispersion. The blank section corresponds to the area not covered by the detector.

with the grooves with respect to the light, α in the grating equation. In other words the grating cannot be precisely rotated about its normal. However, the effect of this error decreases with increasing gamma. The grating was optimized for a gamma of 2.7 degrees instead of 2 degrees. This leads to light being shared by orders adjacent to the blaze direction instead of optimizing light into the theoretical blaze order. By increasing gamma we will be able to maximize the efficiency in first order while minimizing contributions from zero order.

This grating disperses 18.9% of the direct beam into first order, 6.1% into minus first order and 21.1% into zero order for this configuration. Giving a total of 46.1% of the light in the diffraction arc with 25% dispersed. Varying γ to place first order in the blaze constraint should decrease the contribution from zero order and increase the amount of light that is dispersed. These tests are also currently being done.

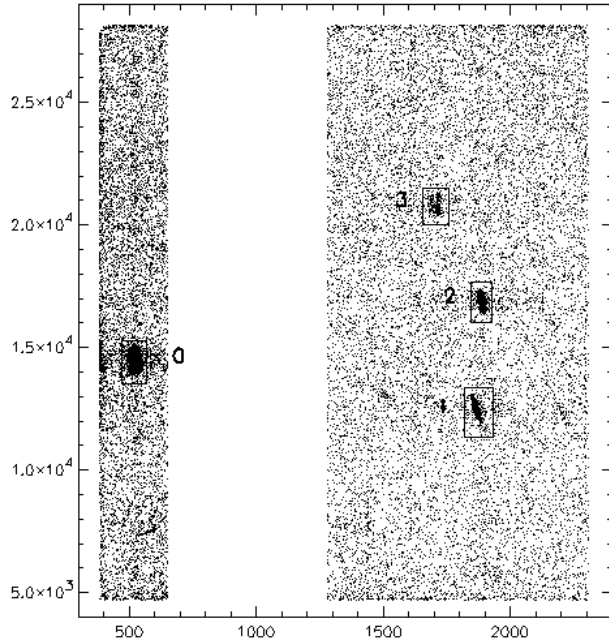


Figure 4: Carbon-K, 0.277keV, data for U3787. Box 0 is the direct beam, box 1 is first order, box 2 is zero order and box 3 is minus first order.

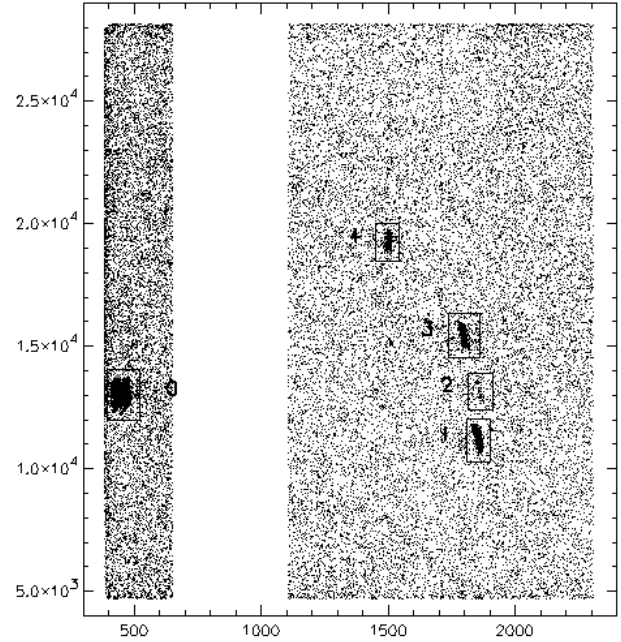


Figure 5: Oxygen-K, 0.525keV, data for U3787. Box 0 is the direct beam, box 1 is second order, box 2 is first order, box 3 is zero order and box 4 is minus second order.

The energy from the Manson source was increased to the Oxygen-K line at 0.525keV by using an oxidized magnesium source. The data are presented in figure 5. Again, box 0 is direct, while box 1 is second order, box 2 is first order, box 3 is zero order and box 4 is minus second order. At this energy and in the identical configuration as the carbon data this grating was 19.6% efficient at second order, 1.5% efficient in first, 6.2% efficient in minus second and 21.6% efficient in zero order. Again the effect of the blaze is seen here. Even though this grating's blaze is optimized for second order at these energies, some first order is seen along the direction of the blaze while minus first order is absent. Additional tests at varying γ are also being done at this energy.

This grating was also tested with Mg-K line at 1.25keV. The U3787 grating displayed scatter in the in-plane dimension as seen in figure 6. This is scatter and not a detector effect because it occurs at several detector positions even if the line isn't in the exposure. At this energy 19.2% is diffracted into 1st order (box 3), 2.65% in second (box 2), 0.32% in third (box 1) and another 3% in minus second (box 4). However, if the in-plane scatter is accounted for in its respective line then the absolute efficiencies are now 31.8% in 1st (box 6) and 5.4% in second (box 7). Note that in this configuration, at this energy, zero order is completely suppressed and only diffracted orders are present. First order is on the blaze and appears as the strongest line. Furthermore, the in-plane scatter is only important in the direction of the blaze. Outside of this horizontal strip there is no scatter. As is evident from figure 6, this scatter does not harm spectral resolution but

there is potential for increased effective area if this scatter could be contained within the line. To improve upon this issue we analyzed gratings taken from upstream in the fabrication process. For instance, we've tested an unblazed grating that has a sinusoidal, holographically ruled groove profile. This grating, denoted CV43D, is identical to U3787 in terms of having radial grooves with a density of 4245 grooves/mm but has not been ion-etched to provide the blazed profile. It simply has the holographically recorded sinusoidal profile. The Mg-K data for this grating is shown in figure 7.

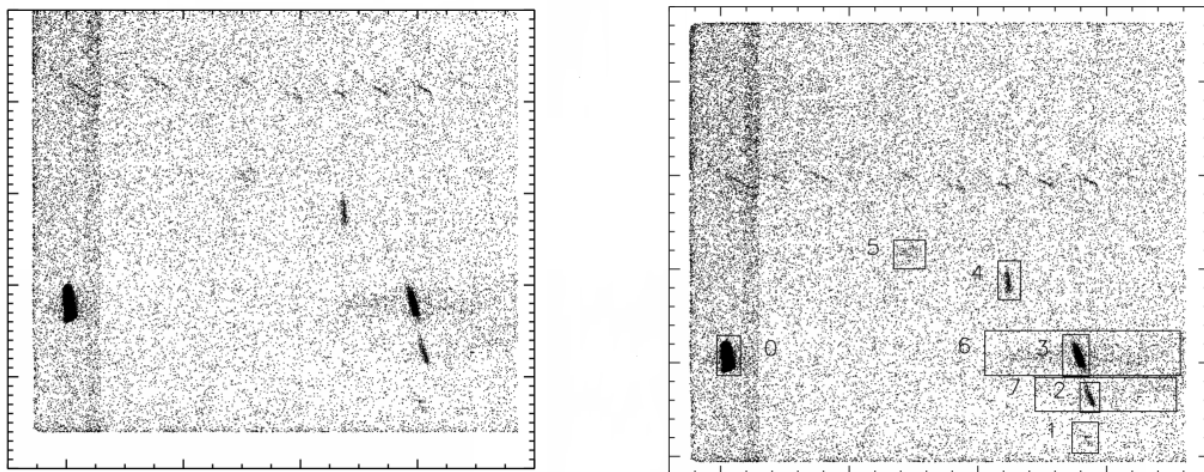


Figure 6: Magnesium-K, 1.25keV, data for U3787. On the left no analysis boxes have been drawn. Note the in-plane scatter that is evident in several of the detector strips. On the right analysis boxes were drawn around both the line itself and the line including scatter. The spots across the top of the image are due to a detector hot spot that appears in each strip.

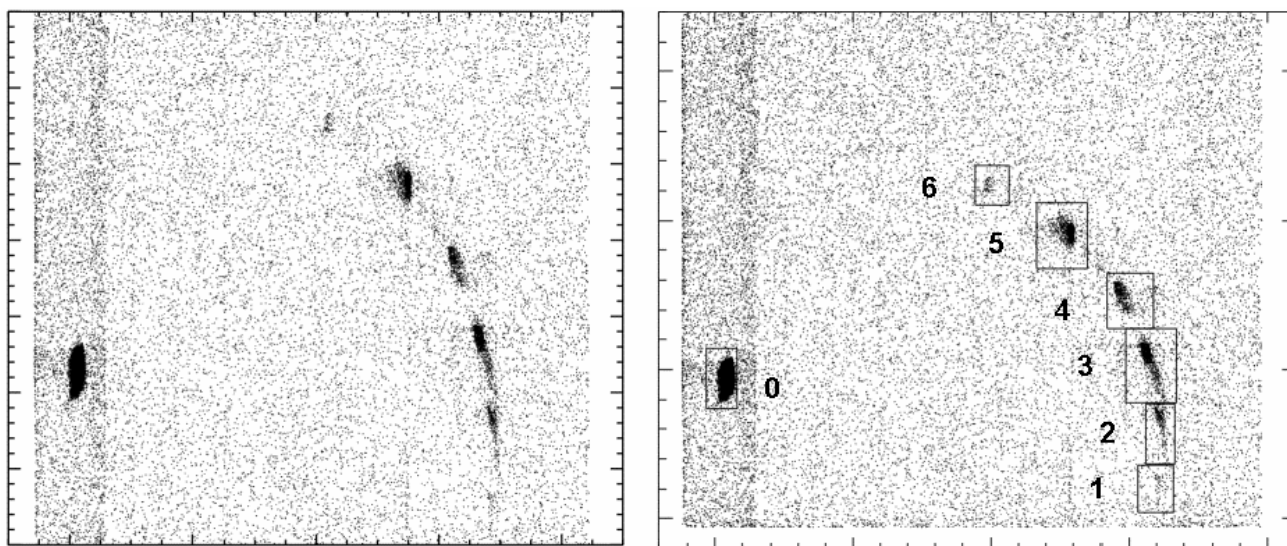


Figure 7: Magnesium-K, 1.25keV, data for CV43D. Note the absence of in-plane scatter. Furthermore, an additional 16.5% of light is seen in the diffraction arc giving this grating a higher overall efficiency than the blazed counterpart.

The absolute efficiencies are as follow: -2nd order = 1.36%, -1st order = 18.37%, 0 order = 7.58%, 1st order = 15.2%, 2nd order = 4.3%, 3rd order = 0.38%. These efficiencies show a 16.5% increase of light in the dispersion arc with no sign of

scatter. The in-plane scatter arises from imperfections in the grating surface. These results suggest that this could arise from the ion-etching process and is currently being investigated. However, when comparing these gratings another possibility was found. The microroughness of the CV43D grating is only 6Å, while that of U3787 is 9Å possibly causing the additional scatter. Furthermore, at all energies and for both gratings the total amount of light in the diffraction arc is ~10% smaller than expected from reflection theory. This also suggests microroughness but in a more isotropic manner. JY is easily capable of polishing grating substrates to the 2Å level and are currently producing masters with this high polish to investigate this possibility.

4. Conclusions

Gratings have been fabricated by Jobin-Yvon with blazed, high density, radial grooves. The first efficiency tests of these gratings in the off-plane mount have provided some very promising numbers. Diffraction efficiencies at Carbon-K 0.277keV are 25% in diffracted orders and 46% total. For Oxygen-K 0.525keV the diffracted orders are 27.3% efficient and 49% total. At Mg-K 1.25keV the blazed grating had all of its light in diffracted orders with 40.5% efficiency. The unblazed grating at this energy had 40% in diffracted orders as well with an additional 7% in zero order.

From this initial study we have obtained diffraction efficiencies up to 40% sum of orders under non-optimal conditions. Further studies will include a complete characterization of these gratings at a range of γ and α angles over the same bandpass to determine the full capability of these gratings. In addition to the efficiency tests we will also be performing spectral resolution tests on these gratings.

Acknowledgments

We wish to thank Brian Gleeson and Ann Shipley for help with this effort. The work was supported by NASA grant NAG5-11850.

References

1. H.D. Tananbaum, N.E. White, J. A. Bookbinder, F. E. Marshall, and F. Cordova, "Constellation X-ray mission implementation concept and science overview," *Proc. Soc. Photo-Opt. Instr. Eng.*, **3765**, 62-72, 1999.
2. R.L. McEntaffer, W. Cash and A. Shipley, "Off-plane gratings for Constellation-X", *Soc. Photo-Opt. Instr. Eng.*, **4851**, 549-556, 2002.
3. W. Cash, "X-ray optics. 2: A technique for high resolution", *Applied Optics*, **30**, 1749-1759, 1991.
4. R. Catura, R. Stern, W. Cash, D. Windt, J.L. Culhane, J. Lappington, K. Barnsdale, "X-ray Objective Grating Spectrograph", *Proc. Soc. Photo-Opt. Instr. Eng.*, **830**, 204-216, 1988.
5. M. Neviere, D. Maystre, W.R. Hunter, "On the use of classical and conical diffraction mountings for XUV gratings", *JOSA*, **68**, 1106-1113, 1978.
6. W. Werner, "X-ray efficiencies of blazed gratings in extreme off-plane mountings", *Applied Optics*, **16**, 2078-2080, 1977.
7. L.I. Goray, "Rigorous efficiency calculations for blazed gratings working in in- and off-plane mountings in the 5-50Å wavelength range", *Proc. Soc. Photo-Opt. Instr. Eng.*, these proceedings.
8. R.L. McEntaffer, F.R. Hearty, B. Gleeson, W. Cash, "X-ray test facility for diffraction gratings", these proceedings.